Journal Pre-proof

One-pot construction of acid phosphatase and hemin loaded multifunctional metal–organic framework nanosheets for ratiometric fluorescent arsenate sensing

Xuechao Xu, Zhijie Luo, Kun Ye, Xiaobo Zou, Xiangheng Niu, Jianming Pan

PII: S0304-3894(20)32397-9

DOI: https://doi.org/10.1016/j.jhazmat.2020.124407

Reference: HAZMAT124407

To appear in: *Journal of Hazardous Materials*

Received date: 16 September 2020
Revised date: 16 October 2020
Accepted date: 24 October 2020

Please cite this article as: Xuechao Xu, Zhijie Luo, Kun Ye, Xiaobo Zou, Xiangheng Niu and Jianming Pan, One-pot construction of acid phosphatase and hemin loaded multifunctional metal–organic framework nanosheets for ratiometric fluorescent arsenate sensing, *Journal of Hazardous Materials,* (2020) doi:https://doi.org/10.1016/j.jhazmat.2020.124407

This is a PDF file of an article that has undergone enhancements after acceptance, such as the addition of a cover page and metadata, and formatting for readability, but it is not yet the definitive version of record. This version will undergo additional copyediting, typesetting and review before it is published in its final form, but we are providing this version to give early visibility of the article. Please note that, during the production process, errors may be discovered which could affect the content, and all legal disclaimers that apply to the journal pertain.

© 2020 Published by Elsevier.

One-pot construction of acid phosphatase and hemin loaded multifunctional metal–organic framework nanosheets for ratiometric fluorescent arsenate sensing

Xuechao Xu,[a,b] Zhijie Luo,[b] Kun Ye,[b] Xiaobo Zou,[a] Xiangheng Niu,[b,*] Jianming Pan[b,*]

[a] School of Food and Biological Engineering, Jiangsu University, Zhenjiang 212013, China

[b] Institute of Green Chemistry and Chemical Technology, School of Chemistry and Chemical Engineering, Jiangsu University, Zhenjiang 212013, China

* Corresponding author. E-mail: niuxiangheng@ujs.edu.cn ;pjm@ujs.edu.cn

Abstract: Exploring high-performance sensors for toxic arsenic detection is highly desired because of its great threat to the environment. Herein, we report a ratiometric fluorescent biosensor based on acid phosphatase and hemin loaded multifunctional Zn-based metal–organic framework (ACP/hemin@Zn-MOF) for high-performance arsenate (As(V)) sensing. ACP/hemin@Zn-MOF is constructed by self-assembly, where hemin exhibits peroxidase-like activity and 2-aminoterephthalic acid ligand endows ACP/hemin@Zn-MOF with an intrinsic fluorescence (452 nm). When ACP/hemin@Zn-MOF catalyzes the oxidation of *o*-phenylenediamine (OPD), fluorescent 2,3-diaminophenazine (DAP) with an emission signal (564 nm) is produced and weakens ACP/hemin@Zn-MOF intrinsic fluorescence (452 nm) due to inner filter effect; after adding ascorbic acid 2-phosphate (AAP), ACP can hydrolyze

AAP and produce ascorbic acid, which competitively suppresses the oxidation of OPD, resulting in the decrease of DAP signal (564 nm) and the recovery of ACP/hemin@Zn-MOF signal (452 nm); when As(V) is added, it irreversibly poisons ACP against hydrolyzing AAP, and the fluorescence signal at 564 nm recovers and the one at 452 nm is suppressed again. High-sensitivity and high-selectivity detection of As(V) (3.33–300 μg L^{-1}) is realized, with a detection limit of 1.05 μg L^{-1}. The biosensor was also successfully employed to detect total arsenic and As(V) in rice.

Graphical abstract

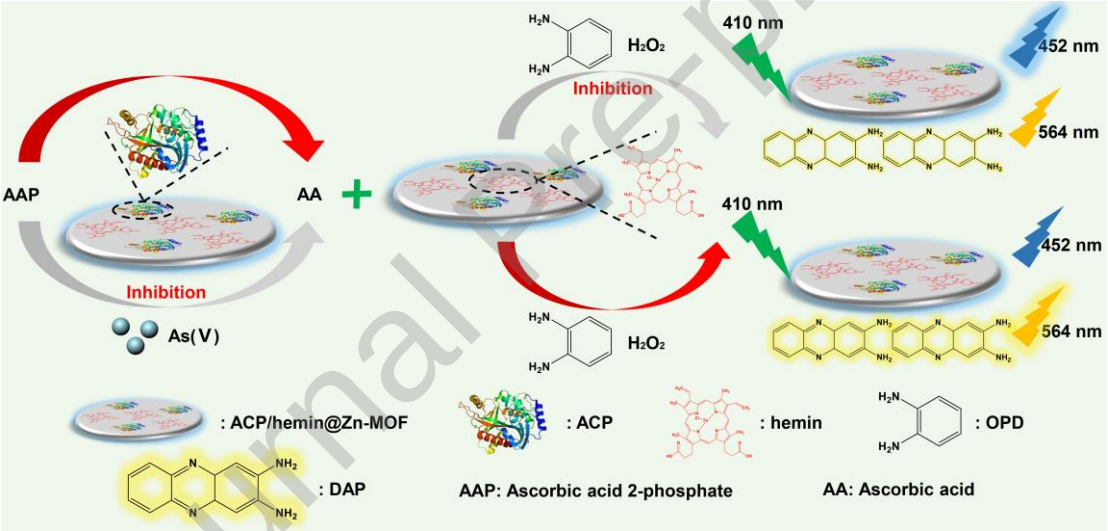

Keywords: Ratiometric fluorescent detection; Arsenate; Nanozyme; Hemin; Acid phosphatase

Journal Pre-proof

1. Introduction

Inorganic arsenic (As) is a serious threat to the survival environment and health security of human due to its extreme toxicity and carcinogenicity [1-3]. High doses of inorganic arsenic can result in skin disease, organ failure, malignant tumor and even death, because it can interact with natural enzymes to influence the physiological processes *in vivo* [4-6]. In consideration of the high dangerousness of inorganic arsenic, many countries and organizations have strictly limited its levels in different matrices. For example, the World Health Organization (WHO) has set the maximum level of inorganic arsenic in drinking water as 10 μg L^{-1}, and China limits the maximum inorganic arsenic content in rice as low as 0.2 mg kg^{-1} [7, 8]. Hence, designing and developing detection methods with high sensitivity, perfect selectivity, and good practicability for inorganic arsenic analysis are extremely urgent.

Up to today, inorganic arsenic detection mainly relies on instrumental methods and biochemical sensors. Although instrumental methods can determine inorganic arsenic selectively and sensitively, they are highly dependent on bulky instruments, tedious operations, and complex pretreatment, which are not conducive to further application of inorganic arsenic detection [9, 10]. Contrastively, biochemical sensors are based on the interactions between inorganic arsenic and signal indicators (optical signals, electrochemical signals, et al.). Thanks to favorable performance, operation ease and miniaturized devices, they have been attracting growing attention [11-13]. However, a common challenge in the field is how to design highly selective sensors for the specific and reliable detection of inorganic arsenic [13], because most of currently

developed sensors are easily disturbed by some interferents, especially phosphate ion [14-16]. Another challenge is to develop sensors with enough sensitivity for low-content analysis. In general, the ratiometric fluorescent strategy is supposed to have the capacity of overcoming the above two problems: on the one hand, ratiometric fluorescent sensors based on the ratio of two fluorescence signals instead of a single signal can provide built-in calibrations to reduce external interferences and improve the detection reliability [17, 18], and on the other hand, the ratio of two fluorescence signals changed upon a stimulus reversely is able to offer amplified readouts for highly sensitive detection [19]. As a result, scientists have been trying to explore ratiometric fluorescent principles and sensors for high-performance arsenic determination [20, 21].

Nanozymes as emerging nanomaterials possess some enzyme-like activities, such as oxidase-like activity and peroxidase-like activity [22, 23]. Due to the favorable properties of high stability, low cost, controllable activity and easy preparation, they are widely utilized for the detection of various targets ranging from ions and small molecules to bioactive species [24-32]. Attractively, nanozyme-based detection is able to amplify signal readouts via catalyzing reactions, beneficial for obtaining enhanced sensitivity [33]. At present, a lot of nanostructured materials are found exhibiting enzyme-mimicking activity, among which metal–organic frameworks (MOFs) attract special attention because of their unique features of tailored porosity and flexible design [34, 35]: (1) the redox metal nodes can act as active sites to catalyze some reactions like natural enzymes; (2) large surfaces and pores benefit the mass transfer

through MOFs; (3) the organic ligands may play roles as optical or electrochemical labels to provide internal signal outputs. Beyond these, MOFs are often employed as carriers to load enzymes or nanozymes efficiently [36-42]. It is found that integration of nanozymes or natural enzymes into MOFs can (1) simplify detection process; (2) enhance the catalytic efficiency of the loaded enzymes or nanozymes; (3) increase the stability of the loaded enzymes or nanozymes (shielding the loaded enzymes or nanozymes from proteolysis and chelating). In this regard, MOF nanozymes can be designed as multifunctional sensing platforms and hold huge potential in the analytical chemistry field [43-47].

In the present work, we propose a ratiometric fluorescent biosensor with acid phosphatase and hemin loaded Zn-based metal–organic framework nanosheets (ACP/hemin@Zn-MOF) as a multifunctional sensing element for high-performance inorganic arsenate (As(V)) determination. As illustrated in Scheme 1, the ACP/hemin@Zn-MOF synthesized through a one-step self-assembly of Zn^{2+} ion, terephthalic acid (BDC), 2-aminoterephthalic acid (NH_2-BDC), acid phosphatase (ACP), and hemin in one pot at room temperature plays multiple roles: (1) the NH_2-BDC ligand enables the material to offer an intrinsic fluorescence at 452 nm; (2) the loaded hemin can act as a peroxidase mimic to catalyze the oxidation of *o*-phenylenediamine (OPD) to 2,3-diaminophenazine (DAP) with an emission fluorescence at 564 nm, which in turn reduces the ACP/hemin@Zn-MOF intrinsic fluorescence (452 nm) because of inner filter effect; (3) the loaded ACP has the ability of hydrolyzing ascorbic acid 2-phosphate (AAP) to produce ascorbic acid (AA),

which has certain reducibility and can competitively inhibit the oxidation of OPD, leading to the suppression of the DAP signal (564 nm) and the recovery of the ACP/hemin@Zn-MOF one (452 nm); (4) if As(V) exists, it can irreversibly poison the loaded ACP against hydrolyzing AAP, and as a result, the fluorescence signal (564 nm) attributed to the oxidation of OPD to DAP recovers and the one (452 nm) of ACP/hemin@Zn-MOF is suppressed again. With the use of the designed multifunctional ACP/hemin@Zn-MOF, a new ratiometric fluorescent sensor was fabricated for inorganic As(V) detection with good sensitivity and excellent specificity. Its reliable application in analyzing As(V) in food samples was also verified.

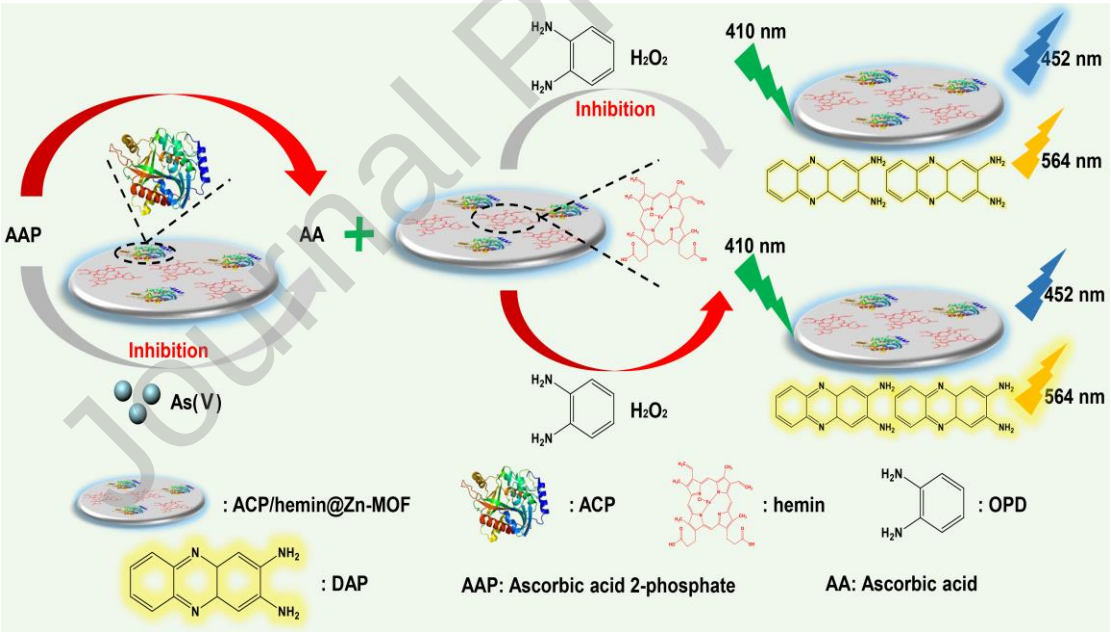

Scheme 1. Illustration of the ratiometric fluorescent detection of inorganic As(V) by using ACP/hemin@Zn-MOF as a multifunctional sensing element.

2. Experimental

2.1. Reagents and One-pot construction and characterization of ACP/hemin@Zn-MOF

The details of reagents, one-pot construction and characterization of ACP/hemin@Zn-MOF are displayed in Supporting Information.

2.2. Peroxidase-like activity and intrinsic fluorescence of ACP/hemin@Zn-MOF

The peroxidase-mimicking feature of ACP/hemin@Zn-MOF was studied by using OPD and H_2O_2 as a substrate couple. All colorimetric and fluorescent measurements were carried out on a Cary 8454 ultraviolet-visible (UV-vis) spectrophotometer (Agilent Technologies) and a F98 fluorescence spectrophotometer (Shanghai Lengguang Technology, China), respectively. Typically, 100 μL ACP/hemin@Zn-MOF (1 mg mL^{-1}, dissolved in deionized water), 100 μL H_2O_2 (9.8 M), and 100 μL OPD (5 mM, dissolved in ethanol) were dispersed in 2700 μL NaAc-HAc buffer (0.2 M, pH 4.0). The reaction was incubated at room temperature for 45 min. After that, the absorbance of the ACP/hemin@Zn-MOF+H_2O_2+OPD system was recorded by UV-vis, and its emission fluorescence signals were recorded by the fluorescence spectrophotometer with an excitation wavelength of 410 nm.

2.3. Ratiometric fluorescent detection of As(V) using ACP/hemin@Zn-MOF

The ratiometric fluorescent detection of As(V) with the use of ACP/hemin@Zn-MOF as a multifunctional sensing element was investigated by the

ACP/hemin@Zn-MOF+H_2O_2+OPD+AAP system. Typically, 100 μL ACP/hemin@Zn-MOF (1 mg mL^{-1}, dissolved in deionized water) and 100 μL As(V) solution (0.1–100 mg L^{-1}) were added to a 5 mL tube and incubated at room temperature for 30 min. Then, 2500 μL NaAc-HAc buffer (0.2 M, pH 4.0) and 100 μL AAP (5 mM) were added to the above mixture and incubated at 37°C for another 30 min. After that, 100 μL H_2O_2 (9.8 M) and 100 μL OPD (5 mM, dissolved in ethanol) were added and incubated at room temperature for further 45 min. The fluorescence of the ACP/hemin@Zn-MOF+H_2O_2+OPD+AAP system with different concentrations of As(V) was recorded by the fluorescence spectrophotometer immediately.

To check the practical application of the fabricated biosensor, it was employed to determine inorganic As(V) and total arsenic in rice samples. The original rice samples collected from Huai'an, China were processed into rice husk, rice bran, unpolished rice, and polished rice. The inorganic As(V) in these samples was extracted by dilute nitric acid, and total arsenic in these samples was obtained by microwave digestion in concentrated nitric acid. After pretreatment, the levels of inorganic As(V) and total arsenic in these samples were tested with a similar process mentioned above. The detailed processes are stated in Supporting Information.

3. Results and discussion

3.1. Fabrication and characterization of ACP/hemin@Zn-MOF

In the present work, ACP/hemin@Zn-MOF is synthesized via a one-pot self-assembly of Zn^{2+} ion, BDC, NH_2-BDC, ACP and hemin at room temperature (Fig. 1A), where

Journal Pre-proof

both BDC and NH_2-BDC with an appropriate ratio (9:1) are employed as organic ligands to coordinate Zn^{2+} ion as well as providing a certain intrinsic fluorescence, and hemin and ACP are loaded into the framework structure to play different catalytic roles. To ensure the successful fabrication of the proposed ACP/hemin@Zn-MOF, it was well characterized by several means. The XRD spectra of pure Zn-MOF and ACP/hemin@Zn-MOF are compared in Fig. 1B. It is found that the XRD spectra of the two materials are generally consistent with that of simulated MOF-5 [48]. Differently, the peak positions of the synthesized Zn-MOF and ACP/hemin@Zn-MOF shift to the left slightly (0.8°). This is because, in comparison with the BDC ligand in simulated MOF-5, the introduction of NH_2-BDC to ACP/hemin@Zn-MOF and pure Zn-MOF slightly increases the distances between interplanar layers [49]. In addition, the consistency of the XRD spectra of ACP/hemin@Zn-MOF with that of Zn-MOF indicates that the loading of ACP and hemin into Zn-MOF has no notable influences on the MOF structure. Fig. S1 (Supporting Information) and Fig. 1C present the microstructures of pure Zn-MOF and ACP/hemin@Zn-MOF prepared. Both Zn-MOF and ACP/hemin@Zn-MOF display nanosheet-like structures. The AFM proofs (Fig. 1D and Fig. S2, Supporting Information) also confirm the sheet-like structures of the two materials. As measured, pure Zn-MOF nanosheets have a diameter of ~600 nm and a thickness of ~150 nm, and the ACP/hemin@Zn-MOF sheets possess a diameter of approximately 250 nm and a thickness of about 50 nm. Apart from size, the synthesized ACP/hemin@Zn-MOF is completely the same as that of Zn-MOF, also suggesting that the loading of ACP and hemin has no notable impacts on the

self-assembly of Zn-MOF. Additionally, the nanosheet-like structures of these materials are supposed to be beneficial to expose rich active sites for catalyzing reactions.

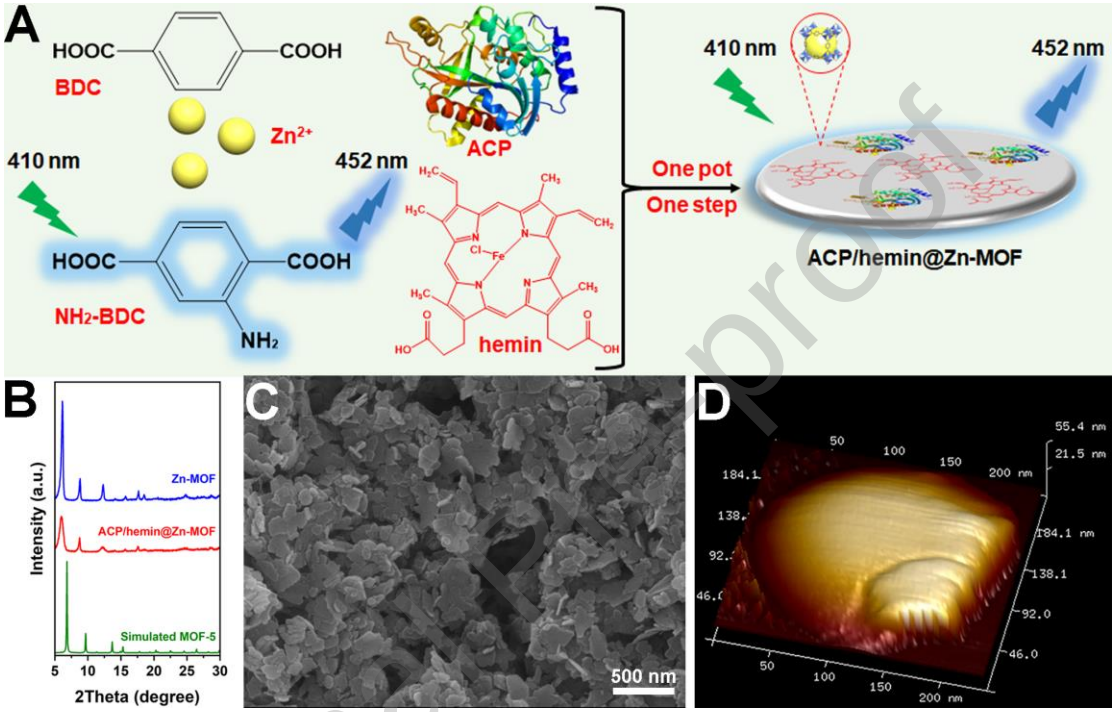

Fig. 1. (A) illustrates the one-pot fabrication of ACP/hemin@Zn-MOF. (B) compares the XRD spectra of Zn-MOF and ACP/hemin@Zn-MOF. (C) and (D) present the SEM and AFM images of ACP/hemin@Zn-MOF nanosheets, respectively.

The surface groups of Zn-MOF and ACP/hemin@Zn-MOF were also investigated. As shown in Fig. 2A, the Fourier transform infrared (FTIR) peaks at 3419 and 1648 cm^{-1} are corresponded to the N–H bond [16], and the weak signal at 1250 cm^{-1} should be ascribed to the stretching vibration of C–N. This proves the presence of the organic ligand NH_2-BDC in ACP/hemin@Zn-MOF. Meanwhile, the FTIR peaks at 1587 and

1379 cm^{-1} are attributed to coordinated carboxyl groups, and the weak signal at 546 cm^{-1} should be ascribed to the Fe–N bond, suggesting the successful loading of hemin. To further confirm the loading of ACP into Zn-MOF, it was labeled with fluorescein isothiocyanate (FITC) and characterized by laser scanning confocal microscopy (LSCM). As displayed in Fig. 2B, both FITC-labeled ACP (green) and NH_2-BDC (blue) in hemin@Zn-MOF are observed. ACP is uniformly distributed in the MOF nanosheets, suggesting that it has been successfully incorporated into Zn-MOF. As displayed in Fig. 2C, the element mapping images of ACP/hemin@Zn-MOF demonstrate the presence of Zn, N, Fe, and S. Among them, the elements Fe and S come from hemin and ACP, respectively, again proving that both hemin and ACP have been integrated into Zn-MOF. Also, the porous features of synthesized Zn-MOF and ACP/hemin@Zn-MOF were studied by N_2 adsorption-desorption isotherms (Fig. 2D), and corresponding physicochemical parameters obtained from N_2 adsorption-desorption measurements are listed in Table S1 (Supporting Information). The specific surface area (S_{BET}) of pure Zn-MOF (40.96 m^2 g^{-1}) is much larger than that of ACP/hemin@Zn-MOF (9.03 m^2 g^{-1}). Moreover, the average pore size of ACP/hemin@Zn-MOF is extremely close to that of pure Zn-MOF. However, the pore volume of ACP/hemin@Zn-MOF is much smaller than that of pure Zn-MOF, indicating that both ACP and hemin were loaded into the pores of Zn-MOF.

Journal Pre-proof

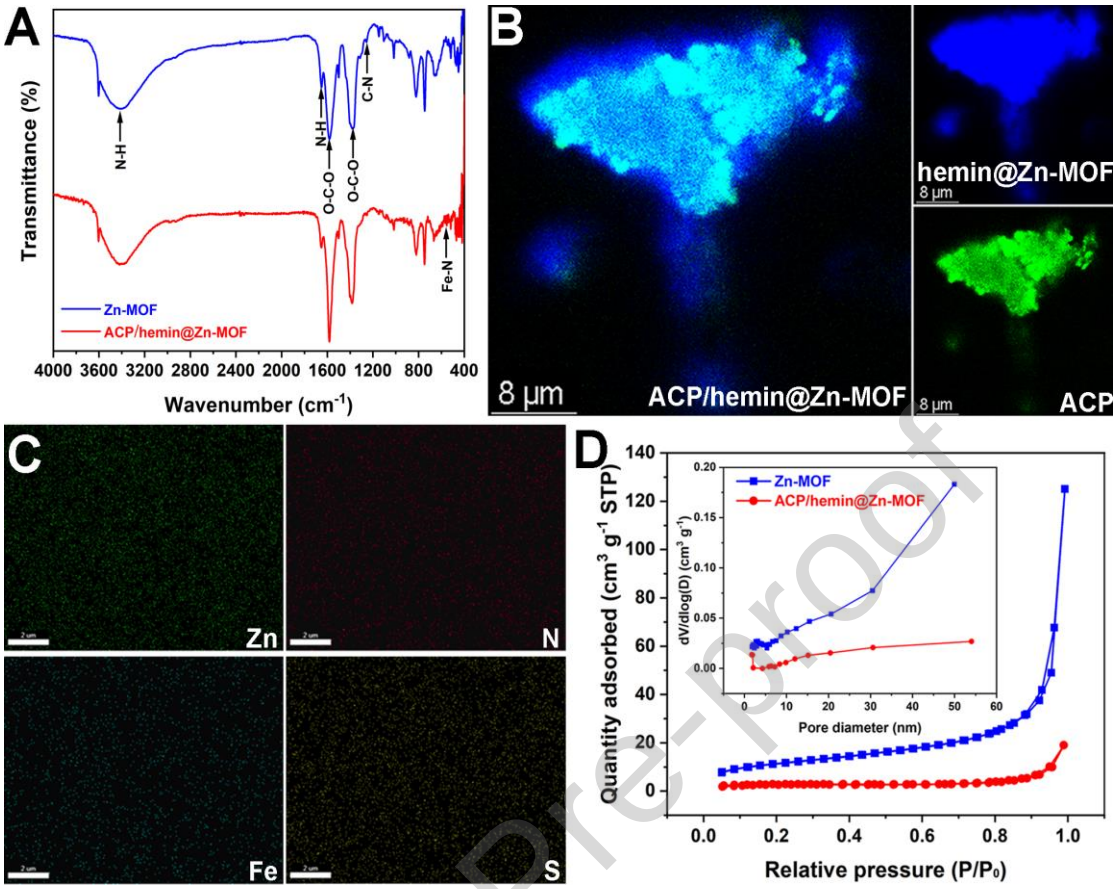

Fig. 2. (A) compares the FTIR spectra of ACP/hemin@Zn-MOF and pure Zn-MOF. (B) shows the LSCM images of ACP/hemin@Zn-MOF, where ACP is labeled with FITC. (C) presents the element mapping of ACP/hemin@Zn-MOF. (D) depicts the N_2 adsorption/desorption isotherms of pure Zn-MOF and ACP/hemin@Zn-MOF, and the inset shows the corresponding pore size distribution plots.

3.2. Peroxidase-like activity and intrinsic fluorescence of ACP/hemin@Zn-MOF

Next, we featured the peroxidase-like activity of ACP/hemin@Zn-MOF by using OPD and H_2O_2 as a peroxidase substrate couple. As demonstrated in Fig. S3A (Supporting Information), in comparison with the ACP/hemin@Zn-MOF+OPD and ACP/hemin@Zn-MOF+H_2O_2 systems, the ACP/hemin@Zn-MOF+H_2O_2+OPD one

exhibits a strong UV-vis absorption peak at ~450 nm, which should originate from the oxidation of the colorless OPD substrate to its yellow oxide called DAP (the inset in Fig. S3A, Supporting Information). This result indicates that the fabricated ACP/hemin@Zn-MOF can act as a peroxidase mimic and catalyze the OPD chromogenic reaction in the presence of H_2O_2. Meanwhile, the time-dependent absorbance changes of these systems (Fig. S3B, Supporting Information) also demonstrate the acceleration role of ACP/hemin@Zn-MOF on the OPD+H_2O_2 chromogenic reaction. To understand the mechanism of the OPD+H_2O_2 chromogenic reaction accelerated by ACP/hemin@Zn-MOF, the possibly generated free radicals were captured by 5,5-dimethyl-1-pyrroline N-oxide (DMPO) and further detected by EPR. As depicted in Fig. S4 (Supporting Information), typical characteristic peaks ascribed to hydroxyl radicals (·OH) are observed. Therefore, it can be inferred that the loaded hemin in ACP/hemin@Zn-MOF plays the peroxidase-like role to catalyze the decomposition of H_2O_2 to generate hydroxyl radicals (·OH), which then oxidize the colorless OPD to yellow DAP (the inset in Fig. S4, Supporting Information).

In addition to the above color changes, the fluorescence spectra of the ACP/hemin@Zn-MOF+H_2O_2+OPD and ACP/hemin@Zn-MOF systems were also collected (Fig. 3A). In ACP/hemin@Zn-MOF, an emission peak at about 452 nm is observed when using 410 nm as an excitation wavelength, which is ascribed to the organic ligand NH_2-BDC in ACP/hemin@Zn-MOF [16, 50]. This indicates that the introduction of NH_2-BDC endows ACP/hemin@Zn-MOF with a remarkable intrinsic fluorescence. After the addition of H_2O_2 and OPD, the ACP/hemin@Zn-MOF

material plays the peroxidase-mimicking role to catalyze the oxidation of OPD to DAP, which can give a notable fluorescence signal at around 564 nm. Interestingly, the intrinsic fluorescence (452 nm) of ACP/hemin@Zn-MOF is suppressed to some extent. To uncover the reason behind the phenomenon observed, both the intrinsic fluorescence signal of ACP/hemin@Zn-MOF and the UV-vis absorption peak of yellow DAP were recorded. As found in Fig. 3B, the ACP/hemin@Zn-MOF emission fluorescence peak at 452 nm significantly overlaps with the UV-vis absorption peak of DAP centered at 450 nm. With this result, inner filter effect (IFE) should be the main reason for the quenching of the ACP/hemin@Zn-MOF intrinsic fluorescence at 452 nm, as illustrated in the inset of Fig. 3B [47].

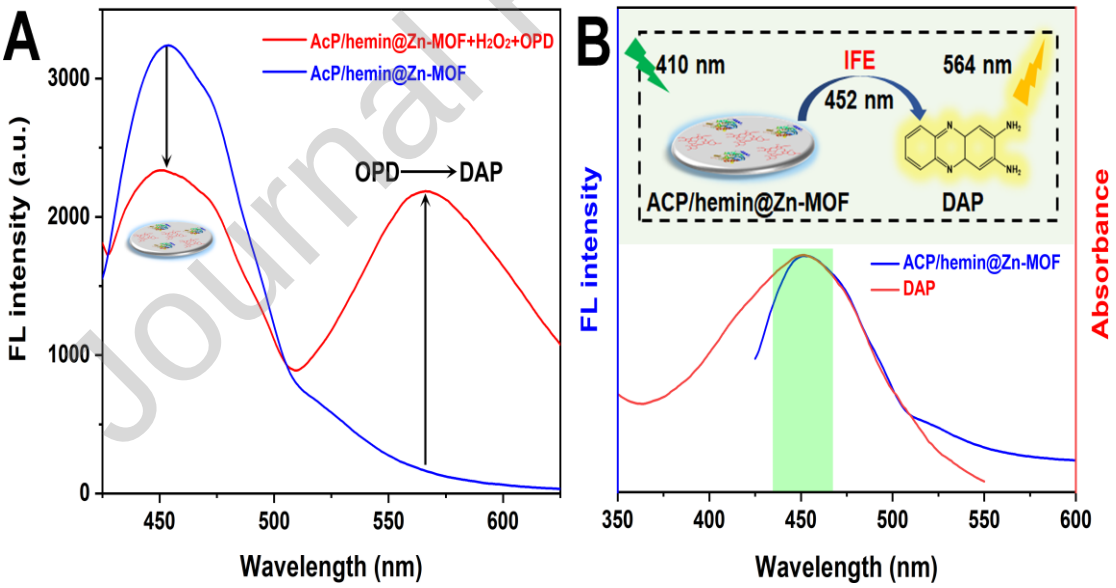

Fig. 3. (A) displays the fluorescence spectra of ACP/hemin@Zn-MOF with the presence of H_2O_2 and OPD or not. (B) uncovers the fluorescence inner filter effect between ACP/hemin@Zn-MOF and the DAP product.

Journal Pre-proof

In addition, the two fluorescence signals at 452 and 564 nm highly depend on the excitation wavelength used. As depicted in Fig. S5 (Supporting Information), the ACP/hemin@Zn-MOF intrinsic fluorescence at 452 nm decreases rapidly with the increase of the excitation wavelength, and the DAP signal at 564 nm almost remains unchanged. Hence, the excitation wavelength is set as 410 nm in the following study. As expected, the two fluorescence peaks given by the ACP/hemin@Zn-MOF+H_2O_2+OPD system change over reaction time. When the reaction time increases, more fluorescent DAP is generated, thus increasing the fluorescence signal at 564 nm and decreasing the one at 452 nm because of IFE (Fig. S6A, Supporting Information). By calculating the fluorescence ratio F_{452}/F_{564}, it decreases along with reaction time until a gradual saturation state appears after 45 min (Fig. S6B, Supporting Information). Thus, the reaction time of ACP/hemin@Zn-MOF and H_2O_2+OPD is selected as 45 min for use.

3.3. Feasibility of ratiometric fluorescent As(V) detection using ACP/hemin@Zn-MOF

Considering that toxic As(V) is able to irreversibly inhibit the catalytic activity of ACP [20, 21, 51], the ACP/hemin@Zn-MOF+H_2O_2+OPD system is supposed to be feasible for detecting As(V). As illustrated in Fig. 4A, with the addition of the AAP substrate, it can be hydrolyzed by the loaded ACP to generate AA, which has certain reducibility and can competitively suppress the formation of DAP catalyzed by the

peroxidase-mimicking hemin loaded in ACP/hemin@Zn-MOF. As a result, the DAP fluorescence peak at 564 nm should decrease, which in turn increases the ACP/hemin@Zn-MOF intrinsic fluorescence at 452 nm due to less IFE. As demonstrated by Fig. 4B, the fluorescence changes of the ACP/hemin@Zn-MOF+H_2O_2+OPD and ACP/hemin@Zn-MOF+H_2O_2+OPD+AAP systems are well consistent with that illustrated in Fig. 4A. After the addition of As(V), it can irreversibly inhibit the catalytic activity of the loaded ACP due to their competitive binding [21]. As a consequence, the AAP substrate cannot be hydrolyzed to produce AA, and such that the OPD oxidation reaction is restored to generate fluorescent DAP. In this regard, the DAP emission fluorescence at 564 nm should increases, which in turn results in the decrease of the ACP/hemin@Zn-MOF intrinsic signal at 452 nm again, as illustrated in Fig. 4C. Also, the fluorescence changes of the ACP/hemin@Zn-MOF+H_2O_2+OPD+AAP and ACP/hemin@Zn-MOF+H_2O_2+OPD+AAP+As(V) systems (Fig. 4D) are the same as the above hypothesis. These results verify that the fabricated ACP/hemin@Zn-MOF indeed can be used as a multifunctional sensing element for the ratiometric fluorescent sensing of As(V).

Journal Pre-proof

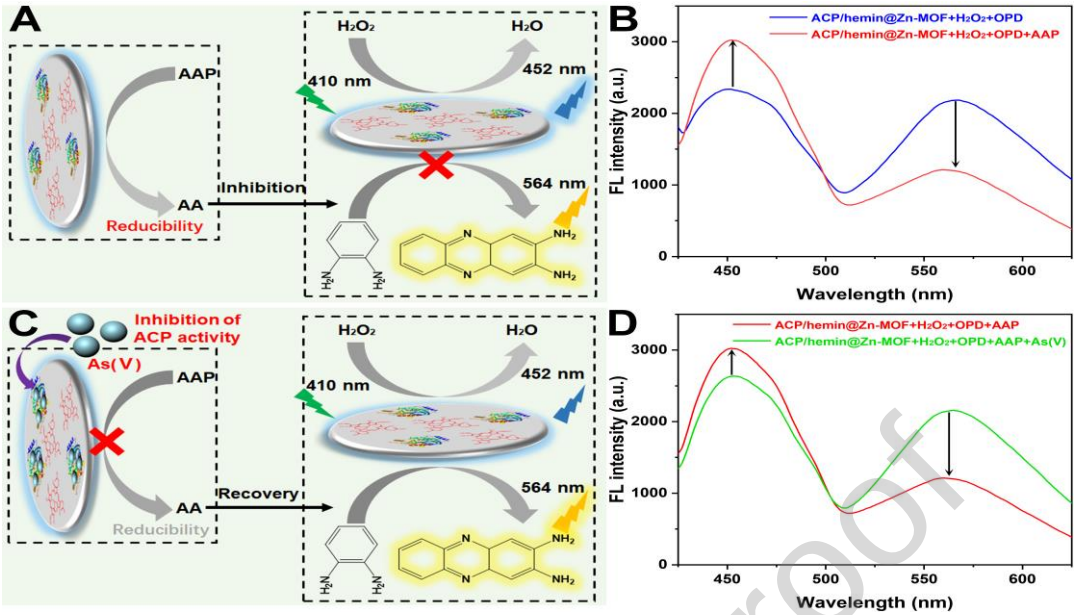

Fig. 4. (A) illustrates that the addition of AAP can impact the fluorescence signals of the ACP/hemin@Zn-MOF+H_2O_2+OPD system, and (B) displays the corresponding spectra. (C) indicates that the presence of inorganic As(V) can affect the fluorescence signals of the ACP/hemin@Zn-MOF+H_2O_2+OPD+APP system, and (D) presents the corresponding spectra.

3.4. High-performance ratiometric fluorescent detection of As(V)

With the above ratiometric fluorescent principle, we further employed the ACP/hemin@Zn-MOF+H_2O_2+OPD+AAP system to detect toxic As(V). To obtain better analytical performance, possible impacts of several parameters, including the amount of AAP used and the reaction time between AAP and ACP, on the fluorescence signals were investigated. As depicted in Fig. S7 (Supporting Information), the fluorescence ratio F_{452}/F_{564} increases along with the increase of AAP concentration and gradually tends to equilibrium. As a consequence, a 166.7 μM concentration of AAP is selected as the optimal amount. As for reaction time, as

presented in Fig. S8 (Supporting Information), the ratio F_{452}/F_{564} also increases with the increase of AAP hydrolysis time, and it gradually reaches to a saturation state after 30 min. Hence, the hydrolysis time of AAP is set as 30 min for As(V) sensing. Under these optimal conditions, the fluorescence spectra of the ACP/hemin@Zn-MOF+H_2O_2+OPD+AAP system with different levels of As(V) were recorded (Fig. 5A). With the increase of As(V) concentration, the ACP/hemin@Zn-MOF intrinsic fluorescence at 452 nm decreases gradually, and the DAP signal at 564 nm increases reversely (Fig. S9, Supporting Information). Furthermore, as depicted in Fig. 5B, the fluorescence ratio F_{452}/F_{564} exhibits a linear decrease dependency on the As(V) level ranging from 3.33 to 300 μg L^{-1}, providing a fitting equation of $F_{452}/F_{564} = -0.0024C_{As(V)} + 2.16$ (R^2=0.997) and a limit of detection (LOD) of 1.05 μg L^{-1} based on S/N = 3. Such a low LOD can fully meet the demands of detecting toxic As(V) in many matrices, as the maximum amount of inorganic arsenic in drinking water is permitted as 10 μg L^{-1}.

Apart from sensitivity, selectivity is also an important parameter for As(V) detection in complex matrices. In our study, 16 kinds of possibly co-existing ions (As(III), Hg^{2+}, Pb^{2+}, Cu^{2+}, Fe^{3+}, Mn^{2+}, Al^{3+}, Na^{+}, Zn^{2+}, Mg^{2+}, SO_4^{2-}, Cl^{-}, CO_3^{2-}, HCO_3^{-}, NO_3^{-} and PO_4^{3-}) were used to study the detection selectivity of the ACP/hemin@Zn-MOF+H_2O_2+OPD+AAP system towards As(V). As can be seen in Fig. 5C and D, these ions, including phosphate ion (Pi), have negligible impacts on the selective detection of As(V) using the ACP/hemin@Zn-MOF+H_2O_2+OPD+AAP system. Such good selectivity should result from the following two aspects: on the

one hand, the loaded ACP can be inhibited by As(V) with excellent specificity [20, 21, 51], and on the other hand, the ratiometric fluorescent sensing mode is able to provide built-in calibrations for external interference elimination. As a result, the fabricated biosensor can offer good selectivity towards As(V) detection. To further highlight the features of our sensor, we compared it with previously reported typical methods for As(V) detection. As listed in Table S2 (Supporting Information), our biosensor based on the ratiometric fluorescent strategy can provide high sensitivity in a wide range with a very low LOD. More attractively, it efficiently resists the interference of Pi with the use of ACP and the ratiometric sensing mode. With these advantages, it holds great potential for the high-performance sensing of toxic As(V).

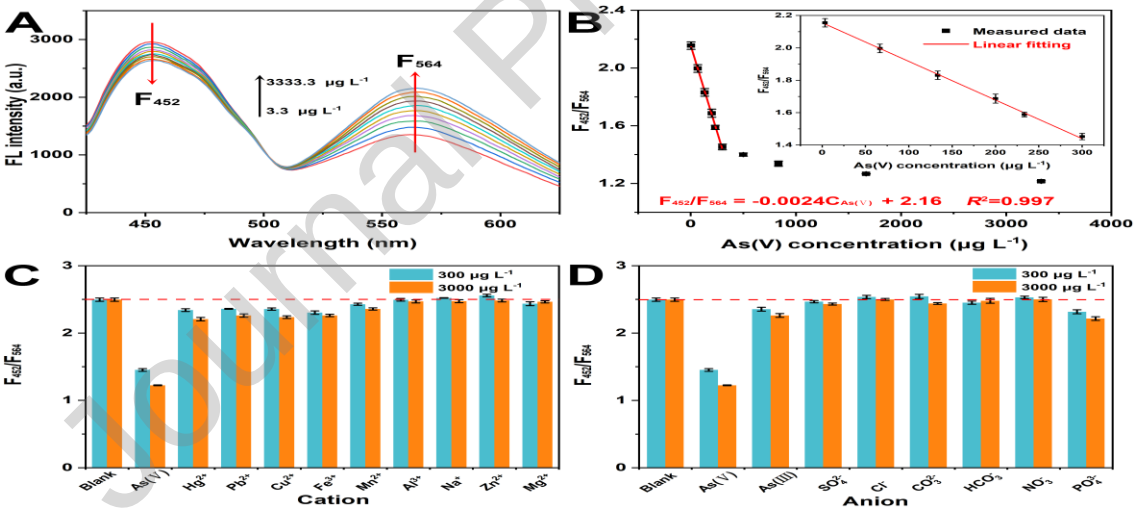

Fig. 5. (A) shows the fluorescence spectra of ACP/hemin@Zn-cMOF+H_2O_2+OPD+AAP with the presence of different levels of As(V), and (B) shows the relationship between the fluorescence ratio F_{452}/F_{564} and the concentration of inorganic As(V). (C) and (D) record the possible effects of commonly coexisting cations and anions on the selective detection of As(V), respectively.

Finally, to check its practicability, we utilized the ACP/hemin@Zn-MOF+H_2O_2+OPD+AAP system to determine inorganic As(V) and total arsenic in rice samples. The detection results (Table 1) show that the recovery rates range from 95% and 105%, indicating that our sensor possesses good detection reliability. Additionally, the detection results determined by our biosensor are well consistent with that detected by ICP-MS, also suggesting its high accuracy. Additionally, the low relative standard deviation of inorganic As(V) detection indicates a good precision of our biosensor. Thus, the biosensor fabricated in the study shows enormous application potential for food and environmental analyses.

Table 1. Detection of total arsenic and inorganic arsenic (As(V)) in rice samples (N = 3).

Target	Sample	Spiked (μg kg^{-1})	Detected (μg kg^{-1})	Recovery rate (%)	ICP-MS (μg kg^{-1})
Total arsenic	Rice husk	–	438.4±21.1	–	455.6±23.1
		200	629.6±24.6	95.6	641.4±32.8
	Rice bran	–	286.5±20.3	–	280.7±17.1
		200	495.9±26.8	104.7	505.2±25.3
	Unpolished rice	–	84.3±15.3	–	80.4±15.4
		200	280.2±24.1	97.9	274.8±20.4
	Polished rice	–	64.8±8.7	–	70.5±10.7
		200	259.4±21.6	97.3	264.1±15.9

Inorganic As(V)	Rice husk	–	416.5±26.4	–	432.1±26.0
		200	619.3±24.1	101.4	627.6±19.3
	Rice bran	–	277.4±18.6	–	262.3±20.5
		200	469.7±7.3	96.2	454.9±23.4
	Unpolished rice	–	74.9±5.8	–	67.1±10.6
		200	279.3±15.9	102.2	261.5±19.7
	Polished rice	–	55.4±10.1	–	56.4±9.4
		200	264.3±16.3	104.5	264.1±15.8

4. Conclusions

To sum up, we have developed a ratiometric fluorescent biosensor for inorganic arsenate detection by using ACP/hemin@Zn-MOF as a multifunctional sensing element. The ACP/hemin@Zn-MOF material fabricated through a one-step self-assembly of precursors in one pot at room temperature plays triple roles: (1) the loaded hemin offers peroxidase-mimicking catalytic activity; (2) the MOF ligand gives an intrinsic fluorescence; (3) the ACP component acts as a specific unit to recognize the analyte As(V). By combining the ACP catalyzed AAP hydrolysis with the hemin catalyzed OPD oxidation, sensing of toxic inorganic As(V) with high sensitivity and excellent selectivity has been realized. Use of the fabricated sensor in analyzing rice samples has also been demonstrated, indicating its potential in practical food and environmental analyses. This work not only provides a new strategy for inorganic As(V) detection with desired performance, but will also inspire the design

and development of integrated bioenzyme/nanozyme platforms with attractive multifunctions for various sensing applications.

Acknowledgements

The work is financially supported by the National Natural Science Foundation of China (No. 21822807 and 21605061), the Natural Science Foundation of Jiangsu Province (No. BK20170323 and BK20170523), the Postgraduate Research & Practice Innovation Program of Jiangsu Province (No. KYCX18_2275), the Key Research and Development Program of Changzhou City (No. CE20195014), the Innovation and Entrepreneurship Program of Jiangsu University (202010299129Y) and the Cultivation Project for Excellent Young Teachers of Jiangsu University (No. 4111310004).

Journal Pre-proof

References

[1] R.N. Ratnaike, Acute and chronic arsenic toxicity, Postgrad. Med. J. 79 (2003) 391-396.

[2] K. Jomova, Z. Jenisova, M. Feszterova, S. Baros, J. Liska, D. Hudecova, C.J. Rhodes, M. Valko, Arsenic: toxicity, oxidative stress and human disease, J. Appl. Toxicol. 31 (2011) 95-107.

[3] A.A. Duker, E.J.M. Carranza, M. Hale, Arsenic geochemistry and health, Environ. Int. 31 (2005) 631-641.

[4] B. Sadee, M.E. Foulkes, S.J. Hill, Coupled techniques for arsenic speciation in food and drinking water: a review, J. Anal. At. Spectrom. 30 (2015) 102-118.

[5] T.S.Y. Choong, T.G. Chuah, Y. Robiah, F.L. Gregory Koay, I. Azni, Arsenic toxicity, health hazards and removal techniques from water: an overview, Desalination 217 (2007) 139-166.

[6] S. Shen, X.-F. Li, W.R. Cullen, M. Weinfeld, X.C. Le, Arsenic Binding to Proteins, Chem. Rev. 113 (2013) 7769-7792.

[7] L. Ma, L. Wang, Y. Jia, Z. Yang, Arsenic speciation in locally grown rice grains from Hunan Province, China: Spatial distribution and potential health risk, Sci. Total Environ. 557-558 (2016) 438-444.

[8] N. Yogarajah, S.S.H. Tsai, Detection of trace arsenic in drinking water: challenges and opportunities for microfluidics, Environ. Sci.: Water Res. Technol. 1 (2015) 426-447.

[9] J. Ma, M.K. Sengupta, D. Yuan, P.K. Dasgupta, Speciation and detection of arsenic in aqueous samples: A review of recent progress in non-atomic spectrometric methods, Anal. Chim. Acta 831 (2014) 1-23.

[10] P. Devi, A. Thakur, R.Y. Lai, S. Saini, R. Jain, P. Kumar, Progress in the materials for optical detection of arsenic in water, TrAC, Trends Anal. Chem. 110 (2019) 97-115.

[11] J. Wei, S.-S. Li, Z. Guo, X. Chen, J.-H. Liu, X.-J. Huang, Adsorbent Assisted in Situ Electrocatalysis: An Ultra-Sensitive Detection of As(III) in Water at Fe_3O_4 Nanosphere Densely Decorated with Au Nanoparticles, Anal. Chem. 88 (2016) 1154-1161.

[12] L. Zeng, D. Zhou, J. Gong, C. Liu, J. Chen, Highly Sensitive Aptasensor for Trace Arsenic(III) Detection Using DNAzyme as the Biocatalytic Amplifier, Anal. Chem. 91 (2019) 1724-1727.

[13] X.C. Xu, X.H. Niu, X. Li, Z.H. Li, D. Du, Y.H. Lin, Nanomaterial-based sensors and biosensors for enhanced inorganic arsenic detection: A functional perspective, Sens. Actuators, B 315 (2020) 128100.

[14] Z. Zhao, Z. Zhang, C. Li, H. Wu, J. Wang, Y. Lu, MOF derived iron oxide-based smart plasmonic Ag/Au hollow and porous nanoshells "ultra-microelectrodes" for ultra-sensitive detection of arsenic, J. Mater. Chem. A 6 (2018) 16164-16169.

[15] A.A. Babu Christus, P. Panneerselvam, A. Ravikumar, Novel, sensitive and selective colorimetric detection of arsenate in aqueous solution by a Fenton-like reaction of Fe_3O_4 nanoparticles, Anal. Methods (2018) 4378-4386.

[16] D. Xie, Y. Ma, Y. Gu, H. Zhou, H. Zhang, G. Wang, Y. Zhang, H. Zhao, Bifunctional NH_2-MIL-88(Fe) metal–organic framework nanooctahedra for highly sensitive detection and efficient removal of arsenate in aqueous media, J. Mater. Chem. A 5 (2017) 23794-23804.

[17] W. Liu, X. Wang, Y. Wang, J. Li, D. Shen, Q. Kang, L. Chen, Ratiometric fluorescence sensor based on dithiothreitol modified carbon dots-gold nanoclusters for the sensitive detection of mercury ions in water samples, Sens. Actuators, B 262 (2018) 810-817.

[18] X. Li, X.H. Niu, P. Liu, X.C. Xu, D. Du, Y.H. Lin, High-performance dual-channel ratiometric colorimetric sensing of phosphate ion based on target-induced differential oxidase-like

activity changes of Ce-Zr bimetal-organic frameworks, Sens. Actuators, B 321 (2020) 128546.

[19] F. Liu, T. Bing, D. Shangguan, M. Zhao, N. Shao, Ratiometric Fluorescent Biosensing of Hydrogen Peroxide and Hydroxyl Radical in Living Cells with Lysozyme–Silver Nanoclusters: Lysozyme as Stabilizing Ligand and Fluorescence Signal Unit, Anal. Chem. 88 (2016) 10631-10638.

[20] S.-H. Wen, R.-P. Liang, H.-H. Zeng, L. Zhang, J.-D. Qiu, CdSe/ZnS quantum dots coated with carboxy-PEG and modified with the terbium(III) complex of guanosine 5′-monophosphate as a fluorescent nanoprobe for ratiometric determination of arsenate via its inhibition of acid phosphatase activity, Microchim. Acta 186 (2019) 45.

[21] Y.-J. Tong, L.-D. Yu, L.-L. Wu, S.-P. Cao, R.-P. Liang, L. Zhang, X.-H. Xia, J.-D. Qiu, Aggregation-induced emission of luminol: a novel strategy for fluorescence ratiometric detection of ALP and As(v) with high sensitivity and selectivity, Chem. Commun. (2018) 7487-7490.

[22] H. Wei, E. Wang, Nanomaterials with enzyme-like characteristics (nanozymes): next-generation artificial enzymes, Chem. Soc. Rev. 42 (2013) 6060-6093.

[23] J. Wu, X. Wang, Q. Wang, Z. Lou, S. Li, Y. Zhu, L. Qin, H. Wei, Nanomaterials with enzyme-like characteristics (nanozymes): next-generation artificial enzymes (II), Chem. Soc. Rev. 48 (2019) 1004-1076.

[24] L. Gao, K. Fan, X. Yan, Iron Oxide Nanozyme: A Multifunctional Enzyme Mimetic for Biomedical Applications, Theranostics 7 (2017) 3207-3227.

[25] Y. Huang, J. Ren, X. Qu, Nanozymes: Classification, Catalytic Mechanisms, Activity Regulation, and Applications, Chem. Rev. 119 (2019) 4357-4412.

[26] Y. Lin, J. Ren, X. Qu, Catalytically Active Nanomaterials: A Promising Candidate for

Artificial Enzymes, Acc. Chem. Res. 47 (2014) 1097-1105.

[27] L. Wang, Z. Hu, S. Wu, J. Pan, X. Xu, X. Niu, A peroxidase-mimicking Zr-based MOF colorimetric sensing array to quantify and discriminate phosphorylated proteins, Anal. Chim. Acta 1121 (2020) 26-34.

[28] X. Niu, Q. Shi, W. Zhu, D. Liu, H. Tian, S. Fu, N. Cheng, S. Li, J.N. Smith, D. Du, Y. Lin, Unprecedented peroxidase-mimicking activity of single-atom nanozyme with atomically dispersed Fe-N-x moieties hosted by MOF derived porous carbon, Biosens. Bioelectron.142 (2019) 111495.

[29] Q. Xue, X. Li, Y. Peng, P. Liu, H. Peng, X. Niu, Polyethylenimine-stabilized silver nanoclusters act as an oxidoreductase mimic for colorimetric determination of chromium(VI), Microchim. Acta 187 (2020) 263.

[30] X. Li, B. Liu, K. Ye, L. Ni, X. Xu, F. Qiu, J. Pan, X. Niu, Highly sensitive and specific colorimetric detection of phosphate by using Zr (IV) to synergistically suppress the peroxidase-mimicking activity of hydrophilic Fe3O4 nanocubes, Sens. Actuators, B 297 (2019) 126822.

[31] S. Wu, D. Guo, X. Xu, J. Pan, X. Niu, Colorimetric quantification and discrimination of phenolic pollutants based peroxidase-like Fe3O4 nanoparticles, Sens. Actuators, B 303 (2020) 127225.

[32] X.H. Niu, Y.F. He, X. Li, H.L. Zhao, J.M. Pan, F.X. Qiu, M.B. Lan, A peroxidase-mimicking nanosensor with Hg2+-triggered enzymatic activity of cysteine-decorated ferromagnetic particles for ultrasensitive Hg2+ detection in environmental and biological fluids, Sens. Actuators, B 281 (2019) 445-452.

[33] X. Xu, L. Wang, X. Zou, S. Wu, J. Pan, X. Li, X. Niu, Highly sensitive colorimetric detection

of arsenite based on reassembly-induced oxidase-mimicking activity inhibition of dithiothreitol-capped Pd nanozyme, Sens. Actuators, B 298 (2019) 126876.

[34] S. Li, X. Liu, H. Chai, Y. Huang, Recent advances in the construction and analytical applications of metal-organic frameworks-based nanozymes, TrAC, Trends Anal. Chem. 105 (2018) 391-403.

[35] W.H. Chen, M. Vázquez-González, A. Kozell, A. Cecconello, I. Willner, Cu^{2+}–Modified Metal–Organic Framework Nanoparticles: A Peroxidase–Mimicking Nanoenzyme, Small 14 (2018) 1703149.

[36] Z. Zhao, Y. Huang, W. Liu, F. Ye, S. Zhao, Immobilized Glucose Oxidase on Boronic Acid-Functionalized Hierarchically Porous MOF as an Integrated Nanozyme for One-Step Glucose Detection, ACS Sustainable Chem. Eng. 8 (2020) 4481-4488.

[37] W. Xu, L. Jiao, H. Yan, Y. Wu, L. Chen, W. Gu, D. Du, Y. Lin, C. Zhu, Glucose Oxidase-Integrated Metal–Organic Framework Hybrids as Biomimetic Cascade Nanozymes for Ultrasensitive Glucose Biosensing, ACS Appl. Mater. Interfaces 11 (2019) 22096-22101.

[38] X. Wu, J. Ge, C. Yang, M. Hou, Z. Liu, Facile synthesis of multiple enzyme-containing metal–organic frameworks in a biomolecule-friendly environment, Chem. Commun. 51 (2015) 13408-13411.

[39] J. Liu, W. Zhang, M. Peng, G. Ren, L. Guan, K. Li, Y. Lin, ZIF-67 as Template Generating and Tuning “Raisin Pudding”-Type Nanozyme with Multiple Enzyme-Like Activities: Toward Online Electrochemical Detection of 3, 4-Dihydroxyphenylacetic Acid in the Living Brains, ACS Appl. Mater. Interfaces 12 (2020) 29631-29640.

[40] L. Wang, Y. Chen, Luminescence-Sensing Tb-MOF Nanozyme for the Detection and

Journal Pre-proof

Degradation of Estrogen Endocrine Disruptors, ACS Appl. Mater. Interfaces 12 (2020) 8351-8358.

[41] H. Fang, M. Duo, Kenry, W. Yuxiang, W. Wenbo, Z. Dan, K. Deling, L. Bin, Metal–Organic Framework as a Simple and General Inert Nanocarrier for Photosensitizers to Implement Activatable Photodynamic Therapy, Adv. Funct. Mater. 28 (2018) 1707519.

[42] H. Cheng, L. Zhang, J. He, W. Guo, Z. Zhou, X. Zhang, S. Nie, H. Wei, Integrated Nanozymes with Nanoscale Proximity for in Vivo Neurochemical Monitoring in Living Brains, Anal. Chem. 88 (2016) 5489-5497.

[43] K. Ye, L. Wang, H. Song, X. Li, X. Niu, Bifunctional MIL-53(Fe) with pyrophosphate-mediated peroxidase-like activity and oxidation-stimulated fluorescence switching for alkaline phosphatase detection, J. Mater. Chem. B 7 (2019) 4794-4800.

[44] S. Li, Y. Hou, Q. Chen, X. Zhang, H. Cao, Y. Huang, Promoting Active Sites in MOF-Derived Homobimetallic Hollow Nanocages as a High-Performance Multifunctional Nanozyme Catalyst for Biosensing and Organic Pollutant Degradation, ACS Appl. Mater. Interfaces 12 (2020) 2581-2590.

[45] X. Li, H. Zhou, F. Qi, X. Niu, X. Xu, F. Qiu, Y. He, J. Pan, L. Ni, Three hidden talents in one framework: a terephthalic acid-coordinated cupric metal-organic framework with cascade cysteine oxidase- and peroxidase-mimicking activities and stimulus-responsive fluorescence for cysteine sensing, J. Mater. Chem. B 7 (2019) 2565-2565.

[46] T.R. Lin, Y.M. Qin, Y.L. Huang, R.T. Yang, L. Hou, F.G. Ye, S.L. Zhao, A label-free fluorescence assay for hydrogen peroxide and glucose based on the bifunctional MIL-53(Fe) nanozyme, Chem. Commun. 54 (2018) 1762-1765.

[47] S. Li, X. Hu, Q. Chen, X. Zhang, H. Chai, Y. Huang, Introducing bifunctional metal-organic

frameworks to the construction of a novel ratiometric fluorescence sensor for screening acid phosphatase activity, Biosens. Bioelectron. 137 (2019) 133-139.

[48] Z. Zhang, Y. Chen, S. He, J. Zhang, X. Xu, Y. Yang, F. Nosheen, F. Saleem, W. He, X. Wang, Hierarchical Zn/Ni-MOF-2 Nanosheet-Assembled Hollow Nanocubes for Multicomponent Catalytic Reactions, Angew. Chem., Int. Ed. 53 (2014) 12517-12521.

[49] M.Y. Ma, H. Noei, B. Mienert, J. Niesel, E. Bill, M. Muhler, R.A. Fischer, Y.M. Wang, U. Schatzschneider, N. Metzler-Nolte, Iron Metal–Organic Frameworks MIL–88B and NH_2–MIL–88B for the Loading and Delivery of the Gasotransmitter Carbon Monoxide, Chem. Eur. J. 19 (2013) 6785-6790.

[50] J. Yang, Y. Dai, X.Y. Zhu, Z. Wang, Y.S. Li, Q.X. Zhuang, J.L. Shi, J.L. Gu, Metal–organic frameworks with inherent recognition sites for selective phosphate sensing through their coordination-induced fluorescence enhancement effect, J. Mater. Chem. A 3 (2015) 7445-7452.

[51] J. Zhang, C.-L. Zhang, S.-H. Yu, Tuning Gold Nanoparticle Aggregation through the Inhibition of Acid Phosphatase Bioactivity: A Plasmonic Sensor for Light-Up Visual Detection of Arsenate (AsV), ChemPlusChem 81 (2016) 1147-1151.

Journal Pre-proof

Table

Table 1. Detection of total arsenic and inorganic arsenic (As(V)) in rice samples (N = 3).

Target	Sample	Spiked ($\mu g\ kg^{-1}$)	Detected ($\mu g\ kg^{-1}$)	Recovery rate (%)	ICP-MS ($\mu g\ kg^{-1}$)
Total arsenic	Rice husk	–	438.4±21.1	–	455.6±23.1
		200	629.6±24.6	95.6	641.4±32.8
	Rice bran	–	286.5±20.3	–	280.7±17.1
		200	495.9±26.8	104.7	505.2±25.3
	Unpolished rice	–	84.3±15.3	–	80.4±15.4
		200	280.2±24.1	97.9	274.8±20.4
	Polished rice	–	64.8±8.7	–	70.5±10.7
		200	259.4±21.6	97.3	264.1±15.9
Inorganic As(V)	Rice husk	–	416.5±26.4	–	432.1±26.0
		200	619.3±24.1	101.4	627.6±19.3
	Rice bran	–	277.4±18.6	–	262.3±20.5
		200	469.7±7.3	96.2	454.9±23.4
	Unpolished rice	–	74.9±5.8	–	67.1±10.6
		200	279.3±15.9	102.2	261.5±19.7
	Polished rice	–	55.4±10.1	–	56.4±9.4
		200	264.3±16.3	104.5	264.1±15.8

Journal Pre-proof

Credit Author Statement

Xuechao Xu, Zhijie Luo, and Kun Ye: Conceptualization and experiment design, Writing - review & editing;

Xiaobo Zou: Experimental section, Data analysis, Writing - original draft preparation, Project administration;

Xiangheng Niu: Data analysis, Writing - review & editing, Project administration;

Jianming Pan: Conceptualization and experiment design, Writing - review & editing, Supervision, Project administration.

Journal Pre-proof

Declaration of interests

☒ The authors declare that they have no known competing financial interests or personal relationships that could have appeared to influence the work reported in this paper.

☐The authors declare the following financial interests/personal relationships which may be considered as potential competing interests:

Journal Pre-proof

Highlights

- Both ACP and hemin were loaded on Zn-MOF nanosheets via a one-step self-assembly.
- ACP/hemin@Zn-MOF acted as a multifunctional platform.
- Arsenate detection was realized by a ratiometric fluorescence strategy.
- Total arsenic and inorganic arsenic from rice samples were successfully detected.

Journal Pre-proof